JOURNAL OF GEOPHYSICAL RESEARCH
May 2004; 109(C5) : NIL_29-NIL_43
http://dx.doi.org/10.1029/2003JC002051

An edited version of this paper was published by AGU.

Nutrient mineralization rates and ratios in the eastern South Atlantic

S. Brea[1*], X. A. Álvarez-Salgado[1], M. Álvarez[1], F. F. Pérez[1], L. Mémery[2], H. Mercier[3], M. J. Messias[4]

[1]Consejo Superior de Investigaciones Científicas, Instituto de Investigacións Mariñas, Vigo, Spain
[2]Laboratoire d'Océanographie Dynamique et de Climatologie, Institut Pierre Simon Laplace, CNRS-IRD-UPMC, Paris, France
[3]Laboratoire de Physique des Océans, CNRS-IFREMER-UBO, IFREMER/Centre de Brest, Plouzané, France
[4]School of Environmental Science, University of East Anglia, Norwich, UK

*: Corresponding author : Tel. +34 986 231930; Fax +34 986 292762 sbrea@iim.csic.es

Abstract: The physical and biogeochemical components of nutrients and inorganic carbon distributions along WOCE line A14 are objectively separated by means of a constrained least-squares regression analysis of the mixing of eastern South Atlantic water masses. Contrary to previous approaches, essentially devoted to the intricate South Atlantic circulation, this work is focused on the effects of circulation on nutrients and carbon biogeochemistry, with special emphasis on the stoichiometry and the rate of mineralization processes. Combination of nutrient and apparent CFC-age anomalies, derived from the mixing analysis, indicate faster mineralization rates in the equatorial (12 × 10−2 μmol P kg−1 yr−1) and subequatorial (5.3 × 10−2 μmol P kg−1 yr−1) than in the subtropical (4.3 × 10−2 μmol P kg−1 yr−1) regime at the South Atlantic Central Water (SACW) depth range. Lower rates are obtained in the Antarctic Intermediate Water (AAIW) domain (3.0 × 10−2 μmol P kg−1 yr−1). Significant variation with depth of O2/C/N/P anomalies indicates preferential mineralization of proteins in thermocline waters, as compared with the reference Redfield composition.

Keywords: water masses; biogeochemical cycles; South Atlantic

1. Introduction

The South Atlantic plays a key role in the World Ocean circulation. It connects the North Atlantic Deep Water (NADW), formed in the Labrador and Nordic Seas, with the Antarctic, Pacific and Indian Oceans, and the Antarctic Intermediate Water (AAIW), Circumpolar Deep Water (CDW) and Weddell Sea Deep Water (WSDW), formed south of 50ºS, with the North Atlantic [*Reid*, 1989; 1996]. The complexity of the South Atlantic deep circulation is partly a consequence of the bottom topography. The Mid–Atlantic Ridge, the Rio Grande Rise and the Walvis Ridge separate the South Atlantic into four major basins, Argentine, Brazil, Angola and Cape Basin connected by the Vema and Hunter Channels, Romanche and Chain Fracture Zones, and Walvis Passage (Figure 1). The large–scale circulation in the surface, central and intermediate water domains is greatly influenced by the South Atlantic climatology [*Peterson and Stramma*, 1991; *Stramma and England*, 1999]. Marked thermohaline fronts separate the equatorial, subequatorial, subtropical and subantarctic biogeochemical provinces of the South Atlantic (Figure 1). Remarkably important are the Subantarctic Front (*SAF*) where AAIW sinks, Subtropical Front (*STF*) that separates the South Atlantic Current (SAC) and the Subtropical Gyre (STG), and the Subtropical/Subequatorial Front (*STSEF*) that indicates the biochemical differences between the subtropical downwelling zone and the subequatorial upwelling zone, in the Eastern South Atlantic.

Over the last 15 years efforts to observe and model the hydrography and circulation of South Atlantic water masses, have included the 'South Atlantic Ventilation Experiment (SAVE)' in the late 80's and the 'World Ocean Circulation Experiment (WOCE)' through the 90's. A WOCE meeting devoted to the South Atlantic in Brest (France), in May 1997, and the dedicated Journal of Geophysical Research special section (104(C9), 1999), constituted a milestone for the advance in the understanding of this complex ocean. However, most efforts have been dedicated to the circulation of the South Atlantic, and biogeochemical tracers (such as nutrients and dissolved oxygen) have just been used to support the interpretations of physical oceanographers [e.g., *Reid*, 1989; *Tsuchiya et al.*, 1994; *Larqué et al*., 1997; *Mémery et al*., 2000].

Most of the recent studies on the chemical oceanography of the South Atlantic have essentially dealt with the capacity of this ocean to sequester the anthropogenic atmospheric CO_2 [e.g., *Gruber*, 1998; *Holfort et al.*, 1998; *Ríos et al.*, 2003]. However, less attention has been paid to the influence of the circulation of the South Atlantic on the patterns of nutrient mineralization rates and stoichiometric ratios. On one hand, some authors consider that nutrient mineralization ratios are essentially constant with depth and basin, suggesting that large, fast–sinking phytogenic materials of Redfield composition exported from the surface ocean are consumed at all depths [e.g., *Anderson and Sarmiento*, 1994]. On the contrary, other authors concluded that there are remarkable changes in the nutrient mineralization ratios of the deep waters that fill the different ocean basins [e.g., *Li et al.*, 2000]. Variation of nutrient mineralization ratios with depth within a given ocean basin have also been suggested, indicating strong fractionation during the mineralization of sinking organic matter [e.g., *Shaffer et al.*, 1999].

The objective of this paper is to discuss on the influence of water mass ventilation, advection and mixing along the Eastern South Atlantic on the variability of nutrient mineralization rates and the relevance of fractionation during organic matter degradation. A constrained least–squares analysis of South Atlantic water types has been performed to separate the role of physical and biogeochemical processes on the distribution of non–conservative tracers (section 2). Then, nutrient mineralization rates and ratios are presented (section 3) and discussed (section 4) for the central, intermediate and deep water domains.

2. Data

WOCE line A14 (Figure 1) was occupied during the first leg of cruise CITHER–3, aboard *R/V* l'Atalante, from 11 January to 16 February 1995. Hydrographic and biogeochemical parameters of the WOCE Hydrographic Programme were measured at 105 full–depth stations from 4ºN to 45ºS, along ~9ºW. Total alkalinity (TA) and pH–NBS measurements were performed every three stations. Total inorganic carbon (C_T) was calculated from TA and pH–NBS using the inorganic carbon system equations and the acid constants of *Mehrbach et al*. [1973]. In addition, C_T was directly measured during the cruise by the coulometric method. Measured and calculated C_T agreed within ±3 μmol kg^{-1}

[*Ríos et al*., 2003]. A general presentation of the cruise and the complete database can be found in volumes 2 and 3 of the CITHER–3 data report [1996, 1998]. The parameters used in the present work (salinity, temperature, dissolved oxygen, nutrients, TA, pH–NBS and CFC–11) were measured using standard methods, which are explained in detail in the data reports.

Ages from CFC distributions are estimated assuming equilibration with the overlying atmosphere at the time of water mass formation [*Warner and Weiss*, 1992]. Although equilibrium can be accepted for central and intermediate waters, this is not the case of deep and bottom waters, where undersaturation can be as large as 60% due to deep mixed layers and cold temperatures [*Wallace and Lazier*, 1988]. Therefore, we have restricted our estimation of apparent ages (τ_{CFC}) to South Atlantic Central Waters (SACW) and Antarctic Intermediate Water (AAIW). τ_{CFC} of any water sample in these domains has been calculated following *Doney and Bullister* [1992]. Reconstructed CFC–11 annual mean dry air mole fractions in the Southern Hemisphere were taken after *Walker et al.* [2000].

3. Mixing analysis

In this study, the water mass structure is solved by means of an Optimum Multiparameter analysis (OMP). OMP inverse methods work on the principle of estimating the linear combination of Source Water Types (SWT) that best describes the composition of a given water sample, minimizing the residuals of a set of tracer mixing equations in a non–negative least squares sense [e.g., *Mackas et al.*, 1987]. A water type is a combination of temperature, salinity, nutrients, oxygen and other tracer values. A water mass is a body of water with a common formation history, having its origin in a particular region of the ocean. If a water type corresponds closely to the properties of a water mass in its source region it is called a Source Water Type [*Tomczak*, 1999]. The solution of the OMP analysis includes two physically realistic constraints: the contributions from all sources must sum up 100%, and all contributions have to be non–negative.

The system of equations can be written as follows:

$$\mathbf{X} \cdot \mathbf{A} = \mathbf{N} + \mathbf{R} \tag{1}$$

where **X** is the SWT contributions matrix**, A** is the SWT characteristics matrix, **N** is the matrix of observational data and **R** is the matrix with the residuals of the fit.

In the present work potencial temperature (θ) and salinity (S) enter the OMP analysis of upper Eastern South Atlantic water masses. SiO_4 and the conservative chemical tracer 'NO' ($NO = O_2 + R_N \times NO_3$; *Broecker*, 1974) have also been included in the analysis of water masses below the thermocline, where the assumption of conservative behaviour is acceptable for both parameters [*Anderson and Sarmiento*, 1994; *Holfort and Siedler*, 2001]. R_N has been set to a constant value of 9.3 mol O_2 mol N^{-1} [*Laws*, 1991; *Anderson*, 1995; *Fraga et al.*, 1998]. Therefore, the set of mixing equations is:

$$\begin{aligned}
&\sum_i x_i \cdot \theta_i = \theta_{obs} + r_\theta \\
&\sum_i x_i \cdot S_i = S_{obs} + r_S \\
&\sum_i x_i \cdot (NO)_i = (NO)_{obs} + r_{NO} \\
&\sum_i x_i \cdot (SiO_4)_i = (SiO_4)_{obs} + r_{SiO4} \\
&\sum_i x_i = 1
\end{aligned} \qquad (2)$$

where θ_i, S_i, $(NO)_i$ and $(SiO_4)_i$ represent the known parameter values of the SWT and θ_{obs}, S_{obs}, $(NO)_{obs}$ and $(SiO_4)_{obs}$ are the observed values of the corresponding properties, with their respective residuals r_θ, r_S, r_{NO} and r_{SiO4}. The last row expresses the condition of mass conservation.

The linear mixing equations for θ, S, SiO_4 and 'NO' were properly made dimensionless and weighted. Normalization is done using the mean and standard deviation (STD) values of θ, S, SiO_4 and 'NO' from the SWT matrix (Table 1). Accordingly, the equations are weighted taking into account the squared ratio of the standard deviation of each parameter in the SWT matrix and the uncertainty of the estimation of that water type parameter (Table 1). We have used the following values: W_θ= 3, W_S= 2, W_{Si}= 2 and W_{NO}= 1. A weight of 100 has been assigned to the mass

conservation equation, *i.e.* we have done the reasonable assumption that the mass is accurately conserved. No covariance between tracers is assumed.

We have restricted our OMP analysis to water samples with $\theta \leq 18$ºC, in order to avoid the non–conservative behaviour of S and θ (mass and heat exchange with the atmosphere) in the surface layer. So the final number of observation points included in the analysis is 2742.

A key step in an OMP analysis is the definition of the SWT matrix, this is the physical and biogeochemical characteristics of the water masses used in the mixing analysis. Water samples within the 12º–18ºC temperature range have been defined as South Atlantic Central Water (SACW). Four water types are necessary to adequately retain the observed SACW variability in the Eastern South Atlantic: the corresponding 12ºC and 18ºC types for the subtropical (SACWT1 and SACWT2) and the subequatorial South Atlantic (SACWE1 and SACWE2). *Gordon and Bosley* [1991] first introduced the differentiation between subtropical and subequatorial SACW. The characteristics of these water types have been defined from a linear regression analysis of S *versus* θ considering all samples along line A14 in the 12º–18ºC temperature range. Following *Poole and Tomczak* [1999], the standard errors in the estimation of these regression equations have been used to compute the uncertainty in the estimation of the water–type characteristics (Table 1).

According to *McCartney* [1977; 1982] Antarctic Intermediate Water (AAIW) is formed north of the Subantarctic Front (SAF) and east of the Drake Passage by ventilation of the Subantarctic Mode Water (SAMW) formed in the Southeast Pacific. Following *Piola and Georgi* [1981], the addition of the colder and fresher Antarctic water found in the Polar Front of the Drake Passage is necessary to create the South Atlantic AAIW. Accordingly, we have defined the AAIW along line A14 as a mixture of two water types: AAIW1 and AAIW2 (Table 1). AAIW1 (the lightest AAIW) coincides with the coldest type of SAMW identified by *Piola and Gordon* [1989] in the Subantarctic Zone and Northern Drake Passage and it constitutes the primary type of AAIW in the South Atlantic. 'NO' and SiO_4 of AAIW1 have been obtained by extrapolation of line A14 data to the corresponding S and θ. The

thermohaline and chemical characteristics of AAIW2 have been taken from the southernmost stations of WOCE line A17 in the Western South Atlantic [*Mémery et al*., 2000].

The mixing of deep waters from the three major oceans (North Pacific, Indian and North Atlantic Deep Water) with Weddell Sea Deep Water forms the Circumpolar Deep Water (CDW) in the Antarctic Circumpolar Current, ACC [*Broecker et al*., 1985; *Poisson and Chen*, 1987; *Onken*, 1995]. This water mass does not ventilate through direct contact with the atmosphere but through mixing with the North Atlantic and Weddell Sea Deep Waters. This explains the high nutrient and low oxygen levels in this water mass. We have considered the thermohaline characteristics of the CDW type in the Drake Passage [*Georgi*, 1981; *Broecker et al*., 1985]. 'NO' and SiO_4 have been obtained again by extrapolation of line A14 data (Table 1). We have considered a unique CDW type rather than the upper (UCDW) and lower (LCDW) CDW described by *Sievers and Nowlin* [1984] along the Drake Passage. The UCDW and LCDW differ from the upper (UCPW) and lower (LCPW) Circumpolar Water observed above and below the NADW in the South Atlantic Ocean [*Reid*, 1989]. In this sense, we leave the OMP analysis free to create the UCPW and LCPW types from our unique CDW type, contrary to other authors [e.g. *Maamaatuaiahutapu et al*., 1992; *Larqué et al.*, 1997] who force UCPW and LCPW types in their OMP analysis.

Wüst [1935] established the three major components —upper, middle and lower— that contribute to the North Atlantic Deep Water (NADW). The three NADW types flow south along the coast of North America to enter the South Atlantic as part of the so–called 'Deep Western Boundary Current (DWBC)' [*Speer and McCartney,* 1991]. Following the classical *Wüst*'s circulation scheme, the upper NADW (UNADW) is characterised by a salinity maximum due to the contribution of Mediterranean Overflow Water. UNADW along A14 can also be traced by a local silicate minimum at the depth of the salinity maximum. *Wüst* [1935] characterised the middle NADW (MNADW), delivered from the central Labrador Sea, by a local brief oxygen maximum below the UNADW salinity maximum. Finally, the lower NADW (LNADW) originates from the overflow spills on the Denmark Strait and the Iceland–Scotland sills. A second brief oxygen maximum has been classically used to trace the meridional evolution of LNADW in the Western South Atlantic [*Wüst*, 1935; *Reid*, 1989; *Tsuchiya et*

al., 1994; *Mémery et al*., 2000]. For the purposes of this work, two NADW types are defined: NADW1 adequately models both the UNADW and MNADW, and NADW2 relates with the LNADW. We take the thermohaline and chemical characteristics of these water types (Table 1) from the northern end of WOCE line A17, at ~7ºN [*Mémery et al*., 2000].

Finally, Weddell Sea Deep Water (WSDW) has been included in the OMP analysis. It derives from the poorly ventilated Weddell Sea Bottom Water, which mixes with the overlying Warm Deep Water in a ratio 1:1 [*Onken*, 1995]. WSDW is a cold, oxygen–poor and nutrient–rich water mass which occupies abyssal depths of the South Atlantic [*Reid*, 1989]. The thermohaline and chemical characteristics of the WSDW type (Table 1) were taken from *Arhan et al.* [1999a] and *Mémery et al.* [2000] in the south–western South Atlantic.

At least *n–1* conservative tracers are needed to solve the mixing of *n* SWT. Conservative mixing equations of θ, S, 'NO' and SiO_4, along with the physical constraint in the OMP, allow the simultaneous analysis of a maximum of five SWT. However, mixing of up to ten water types occurs in the Eastern South Atlantic: a) South Atlantic Central Water (SACW), defined by four water types (warm and cold, subtropical and subequatorial SACW); b) Antarctic Intermediate Water (AAIW), defined by two water types; c) Circumpolar Deep Water (CDW); d) North Atlantic Deep Water (NADW), defined by two water types (upper+middle and lower NADW); and e) Weddell Sea Deep Water (WSDW). To overcome the problem of an underdetermined system of linear mixing equations we have clustered the samples in several mixing groups, following the vertical distribution of water masses in the South Atlantic suggested by *Vanicek and Siedler* [2002]. Figure 2 shows the θ–S diagram for all samples considered in the present OMP analysis together with the thermohaline characteristics of the 10 water types. Upper waters are solved mixing the two subequatorial types of SACW (E1, E2), and the subtropical types (T1, T2). As previously commented, only θ and S have been considered in the OMP analysis of these groups due to the non–conservative behaviour of SiO_4 in thermocline waters, and because R_N ('NO') could not be constant above 400m. Intermediate waters result from the mixing of SACWE2, AAIW1, AAIW2, CDW and NADW1, and SACWT2, AAIW1,

AAIW2, CDW, and NADW1. Deep waters are solved by mixing AAIW1, AAIW2, CDW, NADW1 and NADW2. Finally, bottom waters by CDW, NADW2 and WSDW. Intermediate and deep mixing figures overlap to some extension (Figure 2). Each classification has a total residual, this is, the sum of squared residual from each equation in system (2). The sample is then assigned to the mixing figure with the lowest total residual.

The robustness or stability of the model is tested by numerical perturbation experiments [*Lawson and Hanson*, 1974]. The SWT matrix is modified in the following manner: normally distributed random numbers are multiplied by the uncertainty assigned to each tracer and SWT (Table 1), these numbers are then added to the SWT matrix, to finally resolve the system. A total of 100 perturbations are computed to then calculate the mean and standard deviation (STD) of the solution matrix. This STD gives an estimation of the stability of the system. Table 2 indicates the mean values of the former STD values for each SWT. The mixing model is stable as these mean STD values are low. The SWTs with higher mean STD values are those with less samples in the figures defined with them, AAIW1 and AAIW2.

Once the SWT contributions matrix, **X**, is obtained a back–calculation of θ, S, 'NO' and SiO_4 for each sample was performed:

$$\mathbf{N_{BC}} = \mathbf{X} \cdot \mathbf{A} \tag{3}$$

where $\mathbf{N_{BC}}$ is the matrix of the back–calculated θ, S, 'NO' and SiO_4. The correlation coefficient (r^2) and the standard error of the estimate of the regression of the back–calculated *versus* measured parameters give indications of the goodness of fit or reliability of the proposed mixing model. In our case, r^2 is >0.996 for all the conservative parameters and the standard error of the regression is very low (Table 1), only slightly higher than the measurement error.

The following step is to obtain a SWT characteristics matrix, **A'**, of the non–conservative parameters, e.g. phosphate (PO_4), total inorganic carbon (C_T) corrected for the dissolution of $CaCO_3$ as $C = C_T - ½·(TA + NO_3)$ [*Broecker and Peng*, 1982] and apparent age (τ_{CFC}). Following *Pérez et al.* [1993], **A'** is obtained by a least–squares regression analysis of the measured values of PO_4, C and

τ_{CFC} *versus* the SWT contributions matrix, **X**. The product of matrices **X** and **A'** produces a matrix $\mathbf{N'_{BC}}$ of back–calculated PO_4, C and τ_{CFC} values for each sample. These back–calculated values are compared with the measured values to obtain the PO_4, C and τ_{CFC} residuals (from now on anomalies, Δ), which are independent of the conservative mixing of water masses. Finally, a linear regression analysis of the relationships between ΔPO_4, ΔC and $\Delta\tau_{CFC}$ allow quantification of mineralization ratios and rates in different water masses. In this way, phosphorus mineralization rates have been calculated from ΔPO_4 *versus* $\Delta\tau_{CFC}$ regression slopes [model II; *Sokal and Rolf*, 1995] in the SACW and AAIW domains, where the relatively high CFC–11 levels allow a robust estimation of apparent ages and the equilibration–with–the–atmosphere hypothesis is plausible.

4. Results

Full–depth profiles of the conservative parameters θ, S and 'NO' along line A14 are shown in Figure 3. They allow us to infer the main features of the water masses distribution in the eastern South Atlantic. The meridional evolution of the 13ºC isotherm (Figure 3a) will be used to identify the well–defined zonal circulation east of the Mid Atlantic Ridge, separating the equatorial, subequatorial, subtropical and subantarctic regimes crossed by line A14 (Figure 1). The sharp change in salinity and temperature at about ~2ºC (Figures 2 and 3), the so called 'Two Degree Discontinuity' [*Broecker et al*., 1976], traces the penetration of WSDW (θ < 2ºC) south of 32ºS and at the Equator [*Onken*, 1995; *Mercier and Morin*, 1997]. The conspicuous salinity minimum at 500–1000m, observed all along line A14 (Figure 3b), has been used to trace the spreading of AAIW along the South Atlantic [e.g., *Wüst*, 1935; *Reid*, 1989; *Warner and Weiss*, 1992; *Suga and Talley*, 1995]. The salinity maximum at 2000–3000m has been used to characterise the penetration of NADW [e.g., *Wüst*, 1935; *Reid*, 1989]. The conservative chemical parameter 'NO' also traces the presence of AAIW ('NO' maximum) and NADW ('NO' minimum) along line A14 (Figure 3c) [*Broecker and Takahashi*, 1981]. Silicate (Figure 4a) is the best tracer for water masses of Antarctic origin, mainly UCPW (local maximum at 1000–

2000m) and WSDW (absolute maximum at the bottom south of 32ºS and at the Equator). It contrasts with the low silicate levels of NADW, mainly at the depth range of the NADW1 (Table 1).

Regarding the non–conservative tracers, the most remarkable feature of the PO_4 distribution (Figure 4b) is the absolute maximum at 1000–1400m in the subantarctic and subtropical zones, related with the advection of the nutrient–rich CDW delivered from the ACC. The PO_4 maximum shifts to 600–800m in the subequatorial and equatorial zones, associated to SACW and AAIW. NADW in the eastern South Atlantic is characterised by a local PO_4 minimum, with values <1.4 μmol kg^{-1} at 1600–2400m in the Equator. Finally, the distribution of CFC–11 along A14 (Figure 4c) gives clear indications of eastern South Atlantic water masses ventilation at the time of sampling, early 1995. The highest CFC–11 levels (>3.5 pmol kg^{-1}) are observed in thermocline waters of the subantarctic region. Relatively high levels are also observed in the subantarctic and subtropical zones along the AAIW domain [*Warner and Weiss*, 1992]. The lowest CFC–11 concentrations (<0.02 pmol kg^{-1}) have been recorded in the NADW domain. The entry of the youngest fractions of NADW1 can be traced through a distinct local maximum of >0.02 pmol kg^{-1} at the Equator.

The average water mass proportions chosen by the mixing analysis are presented in Figure 5. The main features of the AAIW, CDW, NADW and WSDW proportions along line A14 can be straightforwardly tracked. The meridional evolution of the depth of maximum AAIW, UCDW and NADW proportions at each sampling station is also presented (dashed lines in Figure 5). WSDW (Figure 5a) is observed in the southern side of the section (>40%), whereas they reduce to<20% at the Equator. We will highlight the effects of the intricate thermocline, intermediate and deep circulation of the Eastern South Atlantic on the ventilation patterns and nutrient mineralization rates and ratios.

4.1. The South Atlantic Central Water (SACW) domain

Following *Ríos et al*. [2003], the meridional evolution of the SACW 13ºC isotherm (Figure 3a) allows one to delimit the equatorial, subequatorial, subtropical and subantarctic regimes imposed by the wind–driven upper ocean circulation of the South Atlantic along line A14 [*Peterson and Stramma*, 1991; *Stramma and England*, 1999]. The Subtropical Front (STF) is situated between 36º and 37ºS,

where the 13ºC isotherm raises abruptly from 250 to 100m (Figure 3a) and the salinity at this isotherm decreases by 0.30 (Figure 6a). South of the STF, line A14 enters the Subantarctic Zone (SAZ), where SACW is absent according to our water types definition (SACW ranges from 12ºC to 18ºC). Finally, line A14 ends at 45ºS, where the temperature distribution denotes the northern end of the Subantarctic Front (SAF).

The most striking feature of the meridional evolution of PO_4 and CFC–11 along the 13ºC isotherm (Figure 6b) is the abrupt change of concentration at 15ºS. It separates the 'young' (CFC–11 >2.5 pmol kg^{-1}) and 'ventilated' (PO_4 <1.0 μmol kg^{-1}) subtropical SACW to the south from the 'old' (CFC–11 <1.5 pmol kg^{-1}) and 'aged' (PO_4 >1.5 μmol kg^{-1}) subequatorial SACW to the north. North of 15ºS, maximum PO_4 values are obtained in the SEG, between 4 and 9ºS. Then, PO_4 decreases within the relatively 'ventilated' SACW transported by the South Equatorial Undercurrent (SEUC; *Mercier et al.*, 2003), at 3–4ºS, and the Equatorial Undercurrent (EUC; *Mercier et al.*, 2003), at the Equator. North of the Equator, PO_4 increases again within the 'aged' SACW transported by the North South Equatorial Current (Figure 1; NSEC; *Mercier et al.*, 2003). South of 15ºS, it should be noticed the abrupt decrease (increase) of PO_4 (CFC–11) south of the STF.

The meridional evolution of ΔPO_4 (phosphate anomaly) in the subtropical SACW (black circles) along the 13ºC isotherm (Figure 6c) parallels the PO_4 distribution, with a steep increase between 22º and 15ºS, that is, in the subtropical branch of the SEC. In the subequatorial SACW (open circles), local ΔPO_4 maxima are observed in the southern part of the SEG and the NSEC, separated by a minimum at the SEUC and EUC, as suggested by the PO_4 distribution (Figure 6b). A salinity difference of ~0.15 maintains along the 12º–16ºC temperature range (Figure 6d) and decreases for temperatures >16ºC, separating the subequatorial and the subtropical SACW.

The linear regression of ΔNO_3 (nitrate anomaly) *versus* ΔPO_4 (Figure 6e) will provide NO_3/PO_4 slopes independent of the mixing of SACW water types, i.e. related only to mineralization process (Table 3). We obtain slopes [model II; *Sokal and Rolf*, 1995] of 17.9±0.4 mol N mol P^{-1} for subtropical SACW (r^2 = 0.94) and 17.7±0.3 mol N mol P^{-1} for subequatorial SACW (r^2 = 0.96). The

linear regression of ΔC (carbon anomaly) *versus* ΔPO_4 (Figure 6f) will provide C/PO_4 slopes for organic matter mineralization in the SACW domain (Table 3). The resultant slopes are 82±6 mol C mol P^{-1} (r^2 = 0.78) and 99±6 mol C mol P^{-1} (r^2 = 0.91) for the subtropical and subequatorial domains, respectively.

4.2. The Antarctic Intermediate Water (AAIW) domain

The dashed line in Figure 5a illustrates the meridional evolution of the maximum proportion of AAIW (X_{AAIW}). It declines from >95% at 45ºS to <50% at 4ºN (Figure 7a). Steep X_{AAIW} reductions are observed at 36–37ºS, 23ºS and 1–2ºS, which mark the presence of the STF, the *STSEF* and the ECS in the AAIW domain, respectively. The steep X_{AAIW} change at 1–2ºS (Figure 7a) relates to the South Intermediate Countercurrent (SICC) described by *Schott et al.* [1995] and recently by *Mercier et al.* [2003]. The meridional evolution of X_{CDW} illustrates how the mixing of these water masses (AAIW and CDW) is utmost in the subequatorial domain (23º–4ºS), where CDW represents ~22% of the water mass along the line of maximum X_{AAIW} (Figure 7a). X_{CDW} increases progressively within the STG to the maximum observed in the SEC and SEG. Finally, X_{CDW} decreases down to ~17% at 3–4ºS and, then, this proportion remains constant in the ECS. The proportion of NADW (X_{NADW}) along the X_{AAIW} maximum (Figure 7a) is null south of 23ºS and remains always <15%, north of this latitude.

Particularly remarkable in Figure 7b is the bi–modal distribution observed in the subequatorial domain (23º–4ºS), with two ΔPO_4 maximum, centred at 20ºS and 10ºS, separated by a local minimum at 15ºS, which coincides with an eastward flow immediately south of 15ºS found by *Mercier et al.* [2003]. On the other hand, the local ΔPO_4 minima centred at 38º–39ºS and 1º–2ºS can be related to the presence of the AAIW transported eastwards by the South Atlantic Current (SAC) and the South and Equatorial Intermediate Countercurrents (SICC, EIC), respectively. The slope of the ΔNO_3 *versus* ΔPO_4 linear regression (r^2= 0.99, n= 103) is 17.1±0.2 mol N mol P^{-1} (Table 3), lower than the N/P ratios obtained in the SACW domain (Figure 7c). Finally, the ΔC *versus* ΔPO_4 linear regression (r^2= 0.99, n= 34) has a slope of 84±2 mol C mol P^{-1} (Figure 7d and Table3).

4.3. The Circumpolar Deep Water (CDW) domain

The dashed line in Figure 5b shows the meridional evolution of the maximum proportion of CDW (X_{CDW}). NADW first meets the CDW coming from the Drake Passage in the South–Western Argentine Basin, at about 50ºS 55ºW [*Reid et al.*, 1977], dividing the CDW in two well defined layers: the upper and lower CPW (UCPW and LCPW). Note that the UCPW spreads northward more than the LCPW: the X_{CDW}= 0.4 isoline extends to 28ºS in the UCPW depth range and to only 37ºS in the LCPW domain. The line of maximum X_{CDW} in Figure 5b is representative for the UCPW.

Maximum X_{CDW} values are observed in the southern side of the section, where it represents up to 66% of the water mass at the depth of maximum CDW proportion (Figure 8a). A marked decrease, from 60% to 50%, is observed in the surroundings of the STF. However, the most remarkable decrease occurs between 28ºS and 23ºS. X_{CDW} reduces from the constant value of 50% in the STG to 32%, as a consequence of the zonal circulation in the Eastern South Atlantic at this latitudinal range [*Arhan et al.*, 2003]. North of 23ºS, NADW is the dominant Deep Water mass in the Eastern South Atlantic and the UCPW appears as a thin core layer centred at 900–1000m up to the northern end of line A14 (Figure 5b). X_{CDW} decreases smoothly from 32% at 23ºS to a minimum of 22% at 4ºN (Figure 8a). It is noticeable that X_{AAIW} rises abruptly at 23ºS. It represents >45% of the water mass along the line of maximum X_{CDW} north of 23ºS, whereas X_{CDW} is <32%. Therefore, we have to emphasise that AAIW is the dominant water mass along the silicate maximum traditionally assigned to CDW.

The meridional evolution of ΔPO_4 (Figure 8b) along the maximum X_{CDW} indicates that the spreading of UCPW is still affected by the complex circulation of the Eastern South Atlantic. The conspicuous bi–modal maximum in the subequatorial domain and the equatorial minimum appear again, although attenuated compared with the AAIW domain. The slope of the ΔNO_3 *versus* ΔPO_4 linear regression (r^2= 0.96, n= 102) is 15.5±0.3 mol N mol P^{-1} (Figure 8c and Table 3). ΔC also correlates with ΔPO_4 (r^2= 0.95, n= 34), with a slope of 80±3 mol C mol P^{-1} (Figure 8d and Table 3).

4.4. The North Atlantic Deep Water (NADW) domain

The dashed line in Figure 5c represents the meridional evolution of the maximum proportion of NADW (X_{NADW}). A core of maximum X_{NADW} values (>98%) is observed in the northernmost side of line A14, centred at 2000m around the Equator. The line of maximum X_{NADW} maintains at a constant depth of ~1900–2000m up to 23ºS, where it suddenly sinks to ~3000m because of the previously referred zonal circulation at this latitudinal range [*Arhan et al.*, 2003]. The distribution of X_{NADW} along the line of maximum NADW proportion (Figure 9a) clearly shows these features. Maximum X_{NADW} (>0.99) are observed between 3ºN and 3ºS, then, X_{NADW} decreases smoothly to 23ºS, where ~10% of NADW is replaced by UCPW. South of 23ºS, X_{NADW} decreases again up to 35ºS, where it is replaced by LCPW.

The main characteristic of the meridional evolution of ΔPO_4 (Figure 9b) is that the range of variation is quite reduced (~0.15 μmol kg^{-1}). Even so, a maximum of ΔPO_4 is observed between 8ºS and 30ºS and the ΔPO_4 decreases north and south of these latitudes. The local equatorial minimum is present again. The slope of the ΔNO_3 *versus* ΔPO_4 linear regression (r^2= 0.69, n= 98) is 12.3±0.7 mol N mol P^{-1} (Figure 9c and Table 3). Finally, the slope of the ΔC *versus* ΔPO_4 linear regression (r^2= 0.64, n= 33) is 80±9 mol C mol P^{-1} (Figure 9d and Table 3).

5. Discussion

5.1. Contrasting organic matter mineralization rates along the Eastern South Atlantic

Comparison of ΔPO_4 and Δage in the SACW (Figure 6c) and AAIW (Figure 7b) domains suggest that phosphorus mineralization presents significant meridional differences within the SACW domain but not within the AAIW domain. A phosphorus mineralization rate of $(12\pm1)\times10^{-2}$ μmol P kg^{-1} yr^{-1} (r^2= 0.84) has been estimated along the SACW 13ºC isotherm from 4ºN to 9ºS (black squares in Figure 10a). From 9ºS to 20ºS (open triangles) the rate decreases to $(5.3\pm0.2)\times10^{-2}$ μmol P kg^{-1} yr^{-1} (r^2= 0.97). Finally, from 21ºS to the STF (open circles) the rate is $(4.3\pm0.5)\times10^{-2}$ μmol P kg^{-1} yr^{-1} (r^2= 0.70). Our results indicate that the high phosphate levels observed in the subequatorial and equatorial

regimes compared with the subtropical regime results not only from longer residence times north of 20ºS (>15 years compared with <10 years) but from faster mineralization rates too. Phosphorus mineralization rate is almost three times greater in the equatorial domain. As suggested by *Reid* [1989], upwelling should be the reason behind these increased mineralization rates. Organic matter mineralization in the oceans is limited by the substrate availability [*Middelburg et al*., 1993], mainly sinking phytogenic materials exported from the photic layer [*Anderson and Sarmiento*, 1994]. Upwelling in the subequatorial and equatorial regimes leads to primary production rates of ~150 g C m^{-2} yr^{-1} [*Longhurst et al.*, 1995] and carbon sinking rates of 60 g C m^{-2} yr^{-1}, assuming an *f*–ratio of 0.4 [*Berger et al*., 1987]. On the contrary, downwelling occurs in the STG, where much lower primary production [~75 g C m^{-2} yr^{-1}; *Longhurst et al.*, 1995] and carbon sinking rates of 7.5 g C m^{-2} yr^{-1} are reported [f – ratio of 0.1; *Berger et al*., 1987]. It should be noticed that although sinking rates are 8 times larger in the subequatorial and equatorial zones than in the subtropical zone, mineralization rates are only 3 times larger in the equatorial zone. This suggests that the velocity of sinking particles in the subequatorial and equatorial regimes is larger than in the subtropical domain, as expected from the contrasting trophic status of upwelling (zooplankton food web; large, rapidly–sinking particles) and downwelling (microbial food web; dissolved organic matter and small, slowly–sinking particles) regimes [e.g. *Legendre and Le Fèvre*, 1989; *Longhurst et al.*, 1995]. Our phosphorus mineralization rates are within the $2–13\times10^{-2}$ μmolP kg^{-1} yr^{-1} range for depths between 100 and 250m that *Shaffer et al*. [1999] have estimated on basis of a fit to sediment trap data for organic C and N and a N/P molar ratio of 16.

In the case of the AAIW domain, CFC–11 values >0.05 pmol kg^{-1} are only observed in the surroundings of the Equator and, mainly, south of 18ºS, along the maximum X_{AAIW} (not shown). ΔPO_4 *versus* Δage within these latitudinal ranges yields a mineralization rate of $(3.02\pm0.08)\times10^{-2}$ μmolP kg^{-1} yr^{-1} (r^2= 0.92) for the AAIW domain (Figure 10b). Unfortunately, phosphorus mineralization rates cannot be calculated in the subequatorial domain because the low CFC–11 concentrations do not allow a robust apparent age calculation. In any case, it should be noticed that the bi–modal distribution

of ΔPO_4 (Figure 7b) suggest that maximum mineralization is unexpectedly observed at the boundary of the subtropical and subequatorial regimes within the SEC (ΔPO_4 maximum centred at 20ºS) rather than within the cyclonic SEG (ΔPO_4 maximum centred at 10ºS). Whereas the local 10ºS maximum is clearly related to the well–documented equatorial and subequatorial oceanic upwelling, the absolute 20ºS maximum seems to be related with the advection of aged AAIW from the Benguela coastal upwelling system. The impact of the Benguela Current on ΔPO_4, producing a bi–modal distribution, is also observed at the level of the UCPW (Figure 8b). In this sense, *Zabel et al*. [1998] and *Hensen et al*. [2000] have observed an intense benthic activity along the continental slope of Namibia and Angola, controlled by the vertical flux of phytogenic organic matter, produced at very high rates (100–400 gC m^{-2} yr^{-1}).

5.2. Fractionation during organic matter mineralization in the Eastern South Atlantic

It has been shown in the results section that $\Delta C/\Delta N/\Delta P$ ratios depend on the study water mass suggesting fractionation during organic matter mineralization in the Eastern South Atlantic. For the case of ΔC, the contribution of the dissolution of anthropogenic CO_2 has to be considered too. Therefore ΔC cannot be used to infer organic matter mineralization ratios at the levels affected by the anthropogenic CO_2 penetration. The stoichiometric model proposed by *Fraga et al.* [1998] was used to infer the fractionation. It is based in the mean composition of each main group of phytoplankton biomolecules, i.e. phosphorus compounds, proteins, lipids and carbohydrates, the oxygen consumed during the oxidation of organic matter, and the corresponding relationships between oxygen consumption and regenerated carbon and nutrients. In Table 4 are summarized the range of possible R_C values and the proportions of phosphorus compounds, proteins, lipids and carbohydrates mineralized at each level (SACW, AAIW, CDW and NADW) obtained considering the computed ΔO_2, ΔN and ΔP ratios and the method proposed by *Fraga et al.* [1998].

The largest deviations from the reference Redfield ratios were observed in the SACW domain, where only θ and S were used to calculate water mass proportions and, therefore, $\Delta O_2/\Delta C/\Delta N/\Delta P$ are completely independent from each other. For the subtropical SACW, we obtain a small range of

possible R_C values, and the composition of the mineralized material is broadly deviated from the reference Redfield composition. With regard to subequatorial SACW, the range of possible R_C values is larger than for subtropical SACW. In any case, Table 4 shows that proteins were mineralized preferably than other compounds in the SACW domain. Moreover, in the subtropical regime the proportion of mineralized proteins is larger than in the subequatorial regime. The smaller size of sinking organic particles (see section 5.1) and, consequently, the larger residence time of these materials, is likely the reason behind the fractionation observed in the subtropical as compared with the subequatorial zone.

In the AAIW, CDW and NADW domains, ΔO_2 and ΔN are not independent because 'NO' is needed to solve the water masses mixing problem. In Table 4 it can be seen a clear decrease in R_P with depth, and, therefore, an increasing mineralisation of phosphorus compounds. The wide range of possible R_C values do not make possible to observe fractionation of the other compounds throughout the water column. Even so, it is remarkable the decrease in the proportion of proteins with depth in relation to the SACW domain. In the level of NADW the $\Delta O_2/\Delta C$ ratio calculated from our data (–1.43) seems not to be affected by the anthropogenic entry of CO_2, and so, the resulting composition would be 16.3% of phosphorus compounds, 46.7% of proteins, 20.8% of lipids and 16.2% of carbohydrates, very similar to the Redfield composition.

The results for SACW fit with the idea that the composition of sinking organic matter is fractionated throughout the water column. The model of *Suess and Müller* [1980] demonstrated that detrital organic matter settling through the water column undergoes strong elemental fractionation by preferential removal of N– and P–containing organic compounds. The studies of *Minster and Boulahdid* [1987] and *Boulahdid and Minster* [1989] about the variation of the R_P ratio from nutrient concentrations along isopycnal surfaces corroborate the idea of fractionation. More recently fractionation has been revisited by *Shaffer et al.* [1999], *Li et al.* [2000] and *Li and Peng* [2002] from the study of nutrient distributions. On the contrary, *Broecker et al.* [1985] and *Peng and Broecker* [1987], and more recently, *Anderson and Sarmiento* [1994], maintain that the mineralization ratios are constant with depth and basin.

Our results suggest that fractionation in the Eastern South Atlantic seems to be due to differences in the lability of compounds during the mineralization of sinking particulate organic matter. Alternative explanations have been suggested by other authors to explain variations in the O_2/C/N/P mineralization ratios in the oceans. *Li and Peng* [2002] detected changes in these ratios in deep waters during its transit from basin to basin along the conveyor belt. In this case fractionation encompasses the progressive ageing of NADW from the North Atlantic to the North Pacific Ocean. For the case of the North Pacific, they suggest that the observed ratios O_2/C/N/P: 162/124/13/1 should be due to denitrification processes in the reducing microenvironments of sinking particles. However, proportions of 10.0% for phosphorus compounds, 30.8% for proteins, 16.0% for lipids and 43.2% for carbohydrates are obtained using the stoichiometric model of *Fraga et al.* [1998], which is just based on the mineralization of organic matter in oxic conditions. The values we get for South Atlantic NADW, with higher proportions of proteins and lower of carbohydrates, confirm the assumption of *Li and Peng* [2002] about changes in remineralization ratios in the global conveyor belt. The results of *Li and Peng* [2002] for other study basins (Atlantic, Southern and Indian Oceans) do not fit into the model of *Fraga et al.* [1998]. Finally, another hypothesis to explain the variation of O_2/C/N/P mineralization ratios are changes associated to anthropogenic effects on biogeochemical cycles, essentially modifications in the quality and quantity of the sinking materials exported from the upper ocean [*Pahlow and Riebesell*, 2000]. However, this hypothesis has been replied by *Gruber et al.* [2000], who proposed that the human impact also affect changes in the source water type properties, and *Zhang et al*. [2000], who claim for the large uncertainties of the systematic corrections applied by *Pahlow and Riebesell* [2000] to the data.

6. Conclusions

Our physical description of the Eastern South Atlantic allows testing the validity of some statements based on the meridional evolution of the extreme values of thermohaline and chemical properties used in the OMP analysis. Some authors have related the silicate maximum at ~1000m in the subequatorial and equatorial domains with a remanent thin core layer of UCPW [e.g., *Reid*, 1989;

McCartney, 1993; *Oudot et al.*, 1999]. Our results confirm that AAIW is the dominant water mass (>45%) at that level, whereas CDW represents <30%, north of 23ºS as suggested by *Larqué et al.* [1997] and *Tsuchiya et al.* [1994].

A novel method for the determination of mineralization rates has been developed combining nutrient and CFC–derived age anomalies at the core of different water masses. The method has been applied to samples where nutrient and CFC–derived age anomalies are robust (the SACW and AAIW domains). Calculated rates vary from 4 to 12 μmol P kg^{-1} yr^{-1} and can be explained in terms of 1) the contrasting characteristics of the different biogeochemical provinces in the Eastern South Atlantic and 2) variation with depth.

Finally, $\Delta O_2/\Delta C/\Delta N/\Delta P$ ratios suggest fractionation during organic matter mineralization in the Eastern South Atlantic. We conclude that proteins are preferably mineralized in the SACW domain, as compared with the reference Redfield composition. The ample range of possible R_C values in the AAIW, CDW and NADW domains allow us to corroborate fractionation only for the case of phosphorus compounds.

Acknowledgements. The authors wish to thank the captain and the crew of *R/V L'Atalante* for their help during the cruise. We are very grateful to M.J. Pazó and T. Rellan for their participation in nutrients, pH and alkalinity measurements. Financial support from this work came from the Spanish 'Comisión Interministerial de Ciencia y Tecnología (CICYT)', contract No. ANT94–1168–E, and from the 'Institut Français de Recherche pour l'exploitation de la Mer (IFREMER)', contract No 94 1430 087. Comments and suggestions from Dr. Oscar Schofield and two anonymous reviewers are highly appreciated and contributed to improve the manuscript.

References

Anderson, L. A., and J. L. Sarmiento, Redfield ratios of remineralization determined by nutrient data analysis, *Global Biogeochem. Cycles*, *8*, 65–80, 1994.

Anderson, L. A., On the hydrogen and oxygen content of marine phytoplankton, *Deep Sea Res.*, *Part I*, *42*, 1675–1680, 1995.

Arhan, M., K. J. Heywood, and B. A. King, The deep waters from the Southern Ocean at the entry of the Argentine Basin, *Deep Sea Res.*, *Part II*, *46*, 475–499, 1999a.

Arhan, M., H. Mercier and Y. –H. Park, On the deep water circulation of the eastern South Atlantic Ocean, *Deep Sea Res.*, *Part I*, *50*, 889–916, 2003.

Berger, W.H., K. Fischer, C. Lai, and G. Wu, Ocean productivity and organic carbon flux. Part I. Overview and maps of primary production and export production. Scripps Institution of Oceanography, Ref. 87–30:1, 1987.

Boulahdid, M., and J. F. Minster, Oxygen Consumption and nutrient regeneration ratios along isopycnal horizons in the Pacific Ocean, *Mar. Chem.*, *26*, 133–153, 1989.

Broecker, W. S., 'NO', a conservative water–mass tracer, *Earth and Planetary Science Letters*, *23*, 100–107, 1974.

Broecker, W. S., T. Takahashi, and Y. –H. Li, Hydrography of the central Atlantic–I. The two–degree discontinuity, *Deep Sea Res.*, *23*, 1083–1104, 1976.

Broecker, W.S., and T. Takahashi, Hydrography of the central Atlantic–IV. Intermediate waters of Antarctic origin, *Deep Sea Res.*, *28*, 177–193, 1981.

Broecker, W.S., and T. –H. Peng, *Tracers in the Sea*, 690 pp., Lamont Doherty Earth Observatory, Palisades, N. Y., 1982.

Broecker, W.S., T. Takahashi, and T. Takahashi, Sources and flow patterns of deep–ocean waters as deduced from potential temperature, salinity and initial phosphate concentration, *J. Geophys. Res.*, *90*, 6925–6939, 1985.

Doney, S.C., and J. L. Bullister, A chlorofluorocarbon section in the eastern North Atlantic, *Deep Sea Res.*, *Part I*, *39*, 1857–1883, 1992.

Fraga, F., A. F. Ríos, F. F. Pérez, and F. G. Figueiras, Theoretical limits of oxygen:carbon and oxygen:nitrogen ratios during photosynthesis and the mineralization of the organic matter in the sea, *Scientia Marina*, *62*, 161–168, 1998.

Georgi, D. T., On the relationships between the large–scale property variations and fine structures of the Antarctic Circumpolar Current, *J. Geophys. Res.*, *86*, 6556–6566, 1981.

Gordon, A. L., Brazil–Malvinas confluence in October 1984, *Deep Sea Res.*, *34*, 359–384, 1989.

Gordon, A. L., and K. T. Bosley, Cyclonic gyre in the tropical south Atlantic, *Deep Sea Res.*, *Part II*, *38*, S323–S343, 1991.

Groupe CITHER–3, Recueil de Données, Campagne CITHER 3, N/O L'Atalante (11 Janvier–2 Avril 1995), vol. 2, CTD–O_2, *Rapport Interne LPO 96–05*, 532 pp., IFREMER/Centre de Brest, Plouzané, France, 1996.

Groupe CITHER–3, Recueil de Données, Campagne CITHER 3, N/O L'Atalante (11 Janvier–2 Avril 1995), vol. 3, Traceurs Géochimiques, *Rapport Interne LPO 98–03*, 586 pp., IFREMER/Centre de Brest, Plouzané, France, 1998.

Gruber, N., Anthropogenic CO2 in the Atlantic Ocean, *Global Biogeochem.* Cycles, 12, 165–191, 1998.

Gruber, N., K. Keller, and R. M. Key, What story is told by oceanic tracer concentrations?, *Science*, *290*, 455–456, 2000.

Hensen, C., M. Zabel, and H. D. Schulz, A comparison of benthic nutrient fluxes from deep–sea sediments off Namibia and Argentina, *Deep Sea Res.*, *Part II*, *47*, 2029–2050, 2000.

Holfort , J., K. M. Johnson, B. Schneider, G. Siedler and D. W. R. Wallace, Meridional transport of dissolved inorganic carbon in the South Atlantic Ocean, *Global Biogeochem. Cycles*, *12*, 479–499, 1998.

Holfort, J., and G. Siedler, The meridional oceanic transport of heat and nutrients in the South Atlantic, *J. Phys. Oceanogr.*, *31*, 5–29, 2001.

Larqué, L., K. Maamaatuaiahutapu, and V. Garçon, On the intermediate and deep water flows in the South Atlantic Ocean, *J. Geophys. Res.*, *102*, 12,425–12,440, 1997.

Laws, E. A., Photosynthetic quotiens, new production and net community production in the open ocean, *Deep Sea Res.*, 38, 143–167, 1991.

Lawson, C.L., and R. J. Hanson, *Solving least squares problems*, Prentice–Hall, Englewood Cliffs, NJ, 1974.

Legendre, L., and J. Le Fèvre, Hydrodynamical singularities as controls of recycled versus export production in oceans, in *Productivity of the Ocean: Present and Past*, edited by W.H. Berger and G. Wefer, pp. 49–63, John Wiley and Sons, Chichester, 1989.

Li, Y. H., D. M. Karl, C. D. Winn, F. T. Mackenzie, and K. Gans, Remineralization ratios in the subtropical north Pacific gyre, *Aquat. Geochem.*, *6*, 65–86, 2000.

Li, Y. H., and T. H. Peng, Latitudinal change of remineralization ratios in the oceans and its implication for nutrient cycles, *Global Biogeochem. Cycles*, *16*, ??–??, 2002.

Longhurst, A., S. Sathyendranath, T. Platt, and C. Caverhill, An estimate of global primary production in the ocean from satellite radiometer data, *J. Plankton Res.*, *17*, 1245–1271, 1995.

Maamaatuaiahutapu, K., V. C. Garçon, C. Provost, M. Boulahdid, and A. P. Osiroff, Brazil–Malvinas confluence: water mass composition, *J. Geophys. Res.*, *97*, 9493–9505, 1992.

Mackas, D.L., K. L. Denman, and A. F. Bennett, Least squares multiple tracer analysis of water mass composition, *J. Geophys. Res.*, *92*, 2907–2918, 1987.

McCartney, M. S., Subantarctic mode water in *A Voyage of Discovery: George Deacon 70th Anniversary Volume*, *Deep Sea Res.*, *24 (Suppl.)*, 103–119, 1977.

McCartney, M. S., The subtropical recirculation of mode waters, *J. Mar. Res.*, *40*, 427–464, 1982.

McCartney, M. S., Crossing of the equator by the deep western boundary current in the western Atlantic Ocean, *J. Phys. Oceanogr.*, *23*, 1953–1974, 1993.

Mémery, L., M. Arhan, X. A. Álvarez–Salgado, M. –J. Messias, H. Mercier, G. C. Castro, and A. F. Ríos, The water masses along the western boundary of the south and equatorial Atlantic, *Progr. Oceanogr.*, *47*, 69–98, 2000.

Mercier, H., and P. Morin, Hydrography of the Romanche and Chain Fracture Zones, *J. Geophys. Res.*, *102*, 10,373–10,389, 1997.

Mercier, H., M. Arhan ,and J. R. E. Lutjeharms, Upper–layer circulation in the eastern Equatorial and South Atlantic Ocean in January–March 1995, *Deep Sea Res.*, *Part I*, *50*, 863–887, 2003.

Middelburg, J. J., T. Vlug, and F. J. W. A. van der Nat, Organic matter mineralization in marine systems, *Global Planet. Change*, *8*, 47–58, 1993.

Minster, J. F., and M. Boulahdid, Redfield ratios along isopycnal surfaces – a complementary study, *Deep Sea Res.*, *34*, 1981–2003, 1987.

Onken, R., The spreading of Lower Circumpolar Deep Water into the Atlantic Ocean, *J. Phys. Oceanogr.*, *25*, 3051–3063, 1995.

Oudot, C., J. F. Ternon, C. Andrié, E. S. Braga, and P. Morin, On the crossing of the equator by intermediate water masses in the western Atlantic Ocean: Indentification and pathways of Antarctic Intermediate Water and Upper Circumpolar Water, *J. Geophys. Res.*, *104*, 20,911–20,926, 1999.

Pahlow, M., and U. Riebesell, Temporal trends in deep ocean Redfield ratios, *Science*, *287*, 831–833, 2000.

Peng, T. H., and W. S. Broecker, C/P ratios in marine detritus, *Global Biogeochem. Cycles*, *1*, 155–161, 1987.

Pérez, F. F., C. Mouriño, F. Fraga, and A. F. Ríos, Displacement of water masses and remineralization rates off the Iberian Peninsula by nutrient anomalies, *J. Mar. Res.*, *51*, 869–892, 1993.

Peterson, R. G., and L. Stramma, Upper–level circulation in the South Atlantic Ocean, *Prog. Oceanogr.*, *26*, 1–73, 1991.

Piola, A., and D. T. Georgi, Sea–air heat and freshwater fluxes in the Drake Passage and Western Scotia Sea, *J. Phys. Oceanogr.*, *11*, 121–126, 1981.

Piola, A. R., and A. L. Gordon, Intermediate waters in the Southwest South Atlantic, *Deep Sea Res.*, *Part II*, *36*, 1–16, 1989.

Poisson, A., and C. T. A. Chen, Why is there little anthropogenic CO_2 in the Antarctic Bottom water?, *Deep Sea Res.*, *Part II*, *34*, 1255–1275, 1987.

Poole, R., and M. Tomczak, Optimum multiparameter analysis of the water mass structure in the Atlantic Ocean thermocline, *Deep Sea Res.*, *Part I*, *46*, 1895–1921, 1999.

Reid, J. L., On the total geostrophic circulation of the South Atlantic Ocean: flow patterns, tracers, and transports, *Prog. Oceanogr.*, *23*, 149–244, 1989.

Reid, J. L., On the circulation of the South Atlantic, in *The South Atlantic: Present and Past Circulation*, edited by G. Wefer et al., pp. 13–44, Springer–Verlag, New York, 1996.

Reid, J. L., W. D. Nowlin Jr., and W. C. Patzert, On the characteristics and circulation of the Southwestern Atlantic Ocean, *J. Phys. Oceanogr.*, *7*, 62–91, 1977.

Ríos, A F., X. A. Álvarez–Salgado, F. F. Pérez, L. S. Bingler, J. Arístegui, and L. Mémery, Carbon dioxide along WOCE line A14: water masses characterization and anthropogenic entry, *J. Geophys. Res.*, *108*, 3123, doi: 10.1029/2000JC000366, 2003.

Schott, F. A., L. Stramma, and J. Fischer, The warm water inflow into the western tropical Atlantic boundary regime, spring 1994, *J. Geophys. Res.*, *100*, 24,745–24,760, 1995.

Shaffer, G., J. Bendtsen, and O. Ulloa, Fractionating during remineralization of organic matter in the ocean, *Deep Sea Res.*, *Part I*, *46*, 185–204, 1999.

Sievers, H. A., and W. D. Nowlin Jr., The stratification and water masses at Drake Passage, *J. Geophys. Res.*, *89*, 10,489–10,514, 1984.

Sokal, R. R., and F. J. Rohlf, Biometry: the principles and practice of statistics in biological research, 3rd edition, W. H. Freeman and Co., 887 pp., 1995.

Speer, K. G., and M. S. McCartney, Tracing Lower North Atlantic Deep Water across the Equator, *J. Geophys. Res.*, *96*, 20,443–20,448, 1991.

Stramma, L., and F. Schott, The mean flow field of the tropical Atlantic ocean, *Deep Sea Res.*, *Part I*, *46*, 279–303, 1999.

Stramma, L., and M. England, On the water masses and mean circulation of the South Atlantic Ocean, *J. Geophys. Res.*, *104*, 20,863–20,883, 1999.

Suess, E., and P. J. Müller, Productivity, sedimentation rate and sedimentary organic matter in the oceans. II. Elemental fractionation, in *Proceedings of the C.N.R.S. Symposium on the Benthic Boundary Layer*, Marseille, France, 17–26, 1980.

Suga, T., and L. D. Talley, Antarctic Intermediate Water circulation in the Tropical and Subtropical South Atlantic, *J. Geophys. Res.*, *100*, 13,441–13,453, 1995.

Tomczak, M., Some historical, theoretical and applied aspects of quantitative water mass analysis, *J. Mar. Res.*, *57*, 275–303, 1999.

Tsuchiya, M., L. D. Talley, and M. S. McCartney, Water–mass distributions in the western South Atlantic; a section from South Georgia Island (54°S) northward across the equator, *J. Mar. Res.*, *52*, 55–81, 1994.

Vanicek, M., and G. Siedler, Zonal fluxes in the deep water layers of the Western South Atlantic Ocean, *J. Phys. Oceanogr.*, *32*, 2205–2235, 2002.

Walker, S. J., R. F. Weiss, and P. K. Salameh, Reconstructed histories of the annual mean atmospheric mole fractions for the halocarbons CFC–11, CFC–12, CFC–113 and carbon tetrachloride, *J. Geophys. Res.*, *105*, 14, 285–14, 296, 2000.

Wallace, D. W. R., and J. R. N. Lazier, Anthropogenic chlorofluoromethanes in newly formed Labrador Sea Water, *Nature*, *332*, 61–63, 1988.

Warner, J. M., and R. F. Weiss, Chlorofluoromethanes in South Atlantic Antarctic Intermediate Water, *Deep Sea Res.*, *Part II*, *39*, 2053–2075, 1992.

Wüst, G., Schichtung und Zirculation des Atlantischen Ozeans, Die Stratosphäre, in *Wissenschaftliche Ergebnisse der Deutschen Atlantischen Expediton auf dem Forschungs– und Vermessungsschiff "Meteor" 1925–1927*, *6*, 180 pp., 1935.

Zabel, M., A Dahmke, and H. D. Schulz, Regional distribution of diffusive phosphate and silicate fluxes through the sediment–water interface: the eastern South Atlantic, *Deep Sea Res.*, *Part I*, *45*, 277–300, 1998.

Zhang, J. Z., C. W. Mordy, L. I. Gordon, A. Ross, and H. E. Garcia, Temporal trends in deep ocean Redfield ratios, *Science*, *289*, 1839a, 2000.

Figure captions

Figure 1. Chart of the South Atlantic Ocean showing the 105 hydrographic stations occupied along WOCE line A14. Major features of the wind–driven upper ocean circulation (100–500m depth range) are shown (adapted from *Stramma and England*, 1999; and *Stramma and Schott*, 1999). The –4000m isobath is also included, to separate the South Atlantic deep basins. **AC**, Agulhas Current; **ACC**, Antarctic Circumpolar Current; **BrC**, Brazil Current; **BeC**, Benguela Current; **EUC**, Equatorial Under Current; **MC**, Malvinas (Falkland) Current; **NBUC**, North Brazil Under Current; **NEC**, North Equatorial Current; **NEUC**, North Equatorial Under Current; **NSEC**, North South Equatorial Current; **SAC**, South Atlantic Current, **SECC**, South Equatorial Counter Current; **SEUC**, South Equatorial Under Current; and **SEC**, South Equatorial Current.

Figure 2. Potential temperature–salinity diagram for all samples considered in this work (n= 2742). The white triangles stands for thermohaline properties of the 10 water types considered in this work.

Figure 3. Full–depth distributions of potential temperature (ºC) (**a**), salinity (**b**) and 'NO' (μmol kg^{-1}) (**c**) along WOCE line A14. **SAF**, Subantarctic Front; **SAZ**, Subantarctic Zone; **STF**, Subtropical Front; **STG**, Subtropical Gyre; **SEC**, Subequatorial Current, **STSEF**, Subtropical–Subequatorial front; **SEG**, Subequatorial gyre; **ECS**, Equatorial Current System.

Figure 4. Full–depth distributions of silicate (**a**), phosphate (**b**) and CFC–11 (**c**) along WOCE line A14. Nutrients in μmol kg^{-1} and CFC–11 in pmol kg^{-1}. **SAF**, Subantarctic Front; **SAZ**, Subantarctic Zone; **STF**, Subtropical Front; **STG**, Subtropical Gyre; **SEC**, Subequatorial Current; **STSEF**, Subtropical–Subequatorial front; **SEG**, Subequatorial gyre; **ECS**, Equatorial Current System.

Figure 5. Full–depth distributions of AAIW and WSDW (**a**), CDW (**b**) and NADW (**c**) proportions along WOCE line A14. **SAF**, Subantarctic Front; **SAZ**, Subantarctic Zone; **STF**, Subtropical Front; **STG**, Subtropical Gyre; **SEC**, Subequatorial Current; **STSEF**, Subtropical–Subequatorial front; **SEG**, Subequatorial gyre; **ECS**, Equatorial Current System. Dashed lines, lines of maximum AAIW, CDW and NADW proportions.

Figure 6. Distribution of hydrographic and geochemical tracers in the SACW domain along WOCE line A14. Meridional variability of salinity (**a**), phosphate (µmol kg^{-1}) and CFC–11 (pmol kg^{-1}) (**b**) and phosphate anomaly (µmol kg^{-1}) and apparent age (years) (**c**) along the reference 13ºC isotherm. Potential temperature *versus* salinity (**d**), nitrate *versus* phosphate anomalies (**e**) and C *versus* phosphate anomalies (**f**) in the 12º–18ºC SACW domain. Open circles, subequatorial SACW; black circles, subtropical SACW. Dashed lines, theoretical N/P:16/1 and C_{org}/P:106/1 ratios.

Figure 7. Distribution of hydrographic and geochemical tracers in the level of AAIW maximum proportion along WOCE line A14. Meridional variability of AAIW, CDW and NADW proportions (**a**), phosphate (µmol kg^{-1}) and apparent age (years) anomalies (**b**), nitrate *versus* phosphate anomalies (µmol kg^{-1}) (**c**) and C *versus* phosphate anomalies (µmol kg^{-1}) (**d**). The thick solid line in panel b shows the 2–degree running–mean of phosphate anomaly. Dashed lines, theoretical N/P:16/1 and C_{org}/P:106/1 ratios.

Figure 8. Distribution of hydrographic and geochemical tracers in the level of CDW maximum proportion along WOCE line A14. Meridional variability of AAIW, CDW and NADW proportions (**a**), phosphate anomaly (µmol kg^{-1}) (**b**), nitrate *versus* phosphate anomalies (µmol kg^{-1}) (**c**) and C *versus* phosphate anomalies (µmol kg^{-1}) (**d**). The thick solid line in panel b shows the 2–degree running–mean of phosphate anomaly. Dashed lines, theoretical N/P:16/1 and C_{org}/P:106/1 ratios.

Figure 9. Distribution of hydrographic and geochemical tracers in the level of NADW maximum proportion along WOCE line A14. Meridional variability of AAIW, CDW and NADW proportions (**a**), phosphate anomaly (µmol kg^{-1}) (**b**), nitrate *versus* phosphate anomalies (µmol kg^{-1}) (**c**) and C *versus* phosphate anomalies (µmol kg^{-1}) (**d**). The thick solid line in panel b shows the 2–degree running–mean of phosphate anomaly. Dashed lines, theoretical N/P:16/1 and C_{org}/P:106/1 ratios.

Figure 10. Phosphate (µmol kg^{-1}) *versus* apparent age (years) anomalies along the SACW 13ºC isotherm (**a**) and the level of AAIW maximum proportion (**b**). In panel a: black squares, 4ºN–9ºS; open triangles, 9ºS–20ºS; open circles, 21ºS–37ºS. In panel b: open circles, 2ºN–2.5ºS and 18.5ºS–45ºS.

Table 1. Matrix of the thermohaline and chemical characteristics of the 10 source water types used in this study of the Eastern South Atlantic water masses: average value ± uncertainty. The adjusted correlation coefficient (r^2), the standard error of the estimate (std. err.) and the number of data (n) of the back–calculated *versus* measured parameters are also presented.

Water type	**Acronyms**	**Temperature** (ºC)	**Salinity**	**'NO'** (μmol kg^{-1})	**Silicate** (μmol kg^{-1})
South Atlantic Central Water subequatorial 1	**SACWE1**	18±0.1	35.90±0.01	262±3	4.0±0.7
South Atlantic Central Water subequatorial 2	**SACWE2**	12±0.1	35.17±0.01	331±3	9.3±0.7
South Atlantic Central Water subtropical 1	**SACWT1**	18±0.16	35.80±0.02	222±4	1.5±0.5
South Atlantic Central Water subtropical 2	**SACWT2**	12±0.16	35.01±0.02	327±4	3.67±0.5
Antarctic Intermediate Water 1	**AAIW1**	4.8±0.08	34.2±0.01	490±3	10.0±0.7
Antarctic Intermediate Water 2	**AAIW2**	3.14±0.08	34.14±0.01	548±3	18.0±0.7
Circumpolar Deep Water	**CDW**	1.6±0.03	34.74±0.003	495±1	96.5±0.9
North Atlantic Deep Water 1	**NADW1**	4.3±0.1	35.008±0.005	429±2	16.1±0.5
North Atlantic Deep Water 2	**NADW2**	2.02±0.03	34.905±0.003	447±1	31.1±0.9
Weddell Sea Deep Water	**WSDW**	–0.2±0.03	34.67±0.001	540±2	135.0±2.0
r^2		0.9998	0.9991	0.9977	0.9995
std. err. of the estimated parameter		±0.048	±0.008	±3	±0.4
n		2742	2742	2742	2742

Table 2. Mean and standard deviation (STD) of the standard deviation values obtained for each SWT contribution after the perturbation analysis. Values expressed as percentages.

SWT	Mean	STD
SACWE1	0.6	0.8
SACWE2	0.4	0.6
SACWT1	0.8	0.7
SACWT2	0.6	0.5
AAIW1	1.0	1.0
AAIW2	1.1	0.9
CDW	0.3	0.2
NADW1	0.5	0.2
NADW2	0.8	0.3
WSDW	0.5	0.04

Table 3. Linear regression of nitrate *versus* phosphate anomalies ($\Delta NO_3/\Delta PO_4$), and carbon *versus* phosphate anomalies ($\Delta C/\Delta PO_4$), for each water type. The errors on the slopes indicate 95% confidence intervals.

Water Type	**$\Delta NO_3/\Delta PO_4$**	**$\Delta C/\Delta PO_4$**
SACWE	17.7±0.3	99±6
SACWT	17.9±0.4	82±6
AAIW	17.1±0.2	84±2
CDW	15.5±0.3	80±3
NADW	12.3±0.7	80±9

Table 4. Stoichiometric coefficients and proportions of mineralized materials for each water type as obtained with the method of Fraga *et al.* (1998) for different water masses along line A14. %P, proportion of mineralized phosphorus compounds; %Prot, proportion of mineralized proteins; %Lip, proportion of mineralized lipids; %Cbh, proportion of mineralized carbohydrates.

	R_C	R_N	R_P	%P	%Prot	%Lip	%Cbh
Redfield	1.41	9.3	149	12.1	47.8	17.5	22.7
SACWE	1.38–1.50	7.9	140	11.5–14.2	51.6–63.6	2.2–19.9	34.8–2.3
SACWT	1.54–1.55	6.1	109	17.0–17.2	77.1–78.3	1.5–2.7	4.5–1.8
AAIW	1.30–1.47	9.3	158	9.4–12.8	39.8–54.4	1.2–28.5	49.6–4.3
CDW	1.30–1.47	9.3	142	10.4–14.2	39.0–53.2	1.2–28.4	49.4–4.3
NADW	1.30–1.47	9.3	114	12.8–17.5	37.0–50.3	1.2–28.1	49.0–4.1

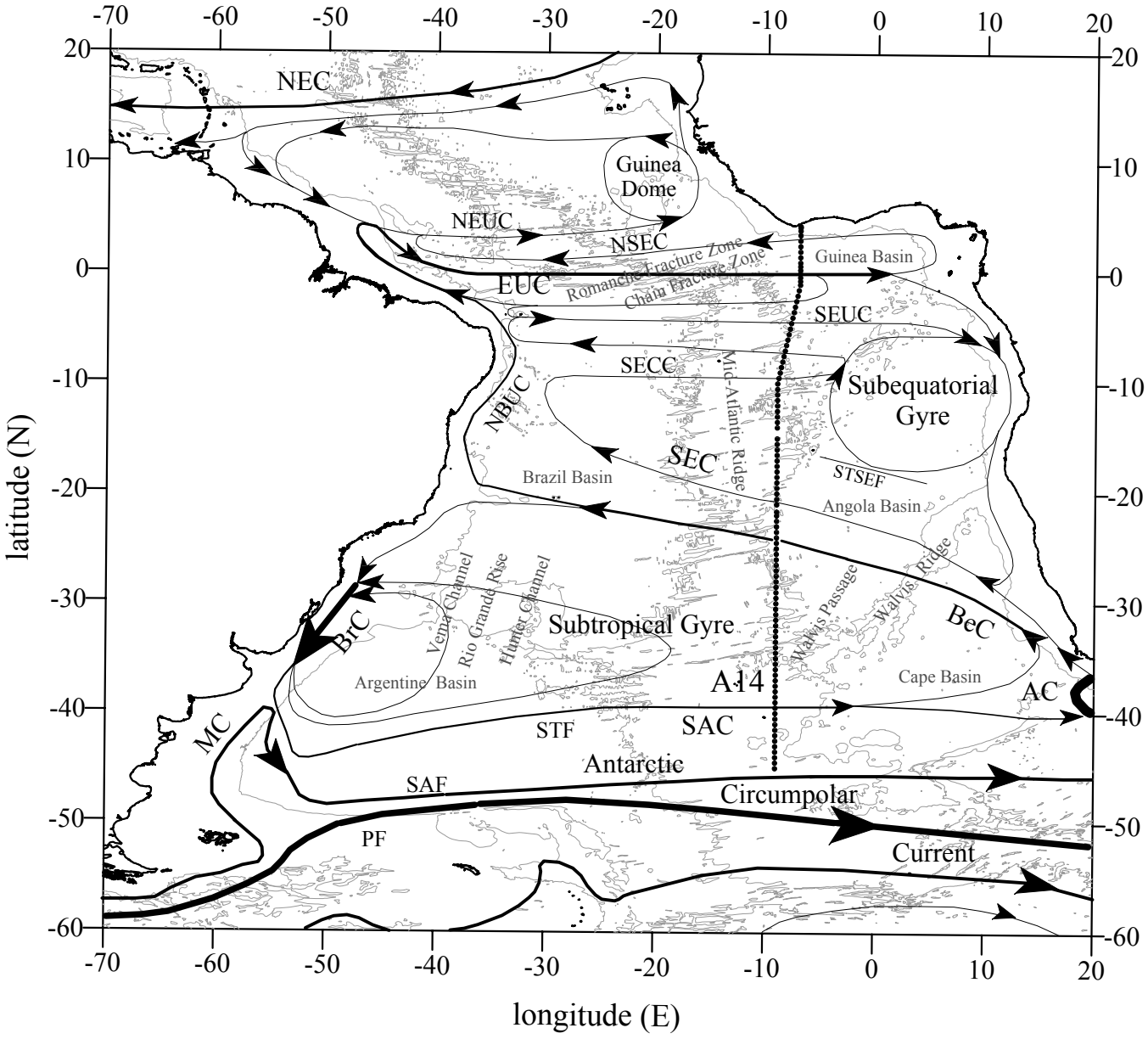

Brea et al., Figure 1

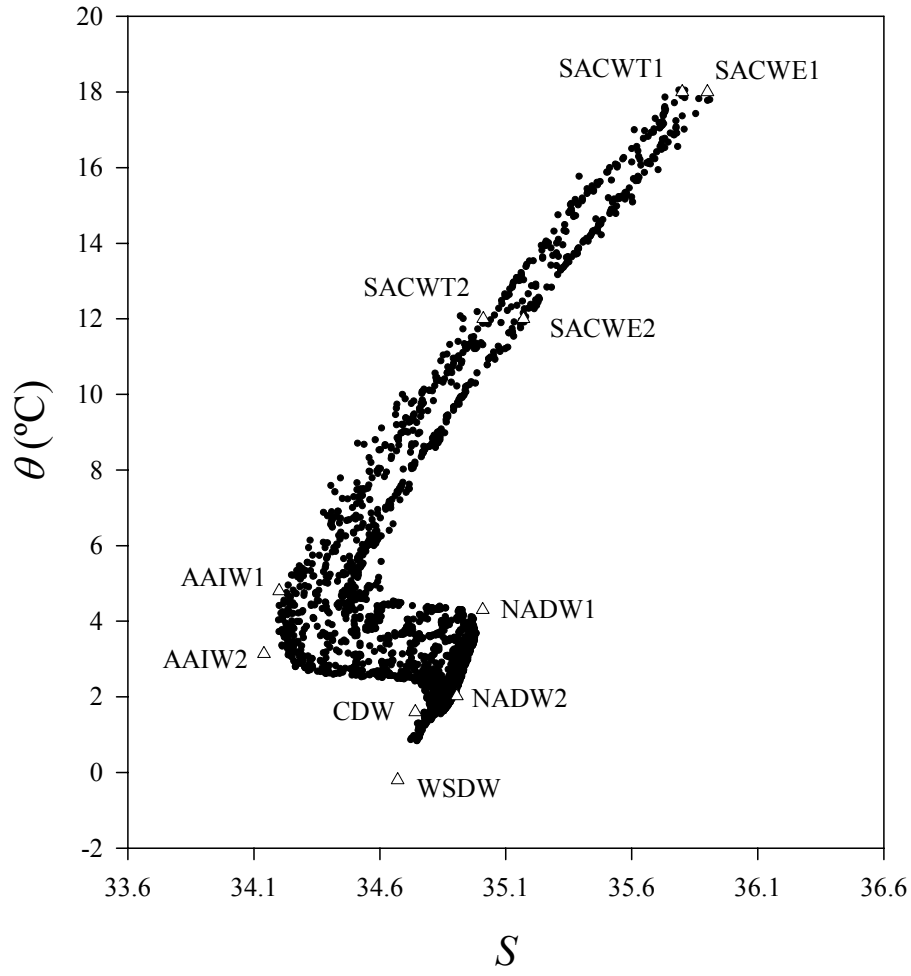

Brea et al., Figure 2

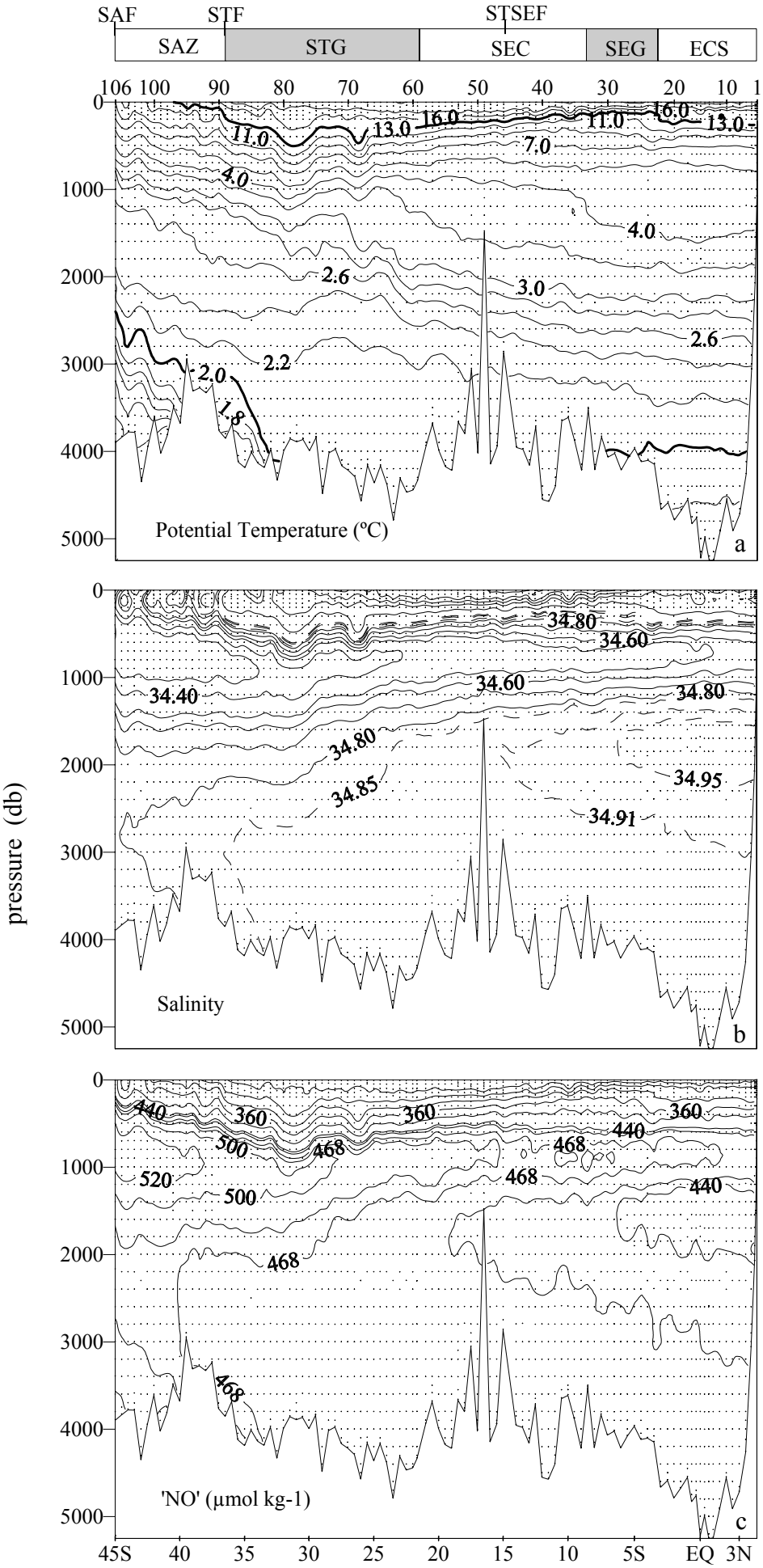

Brea et al., Figure 3

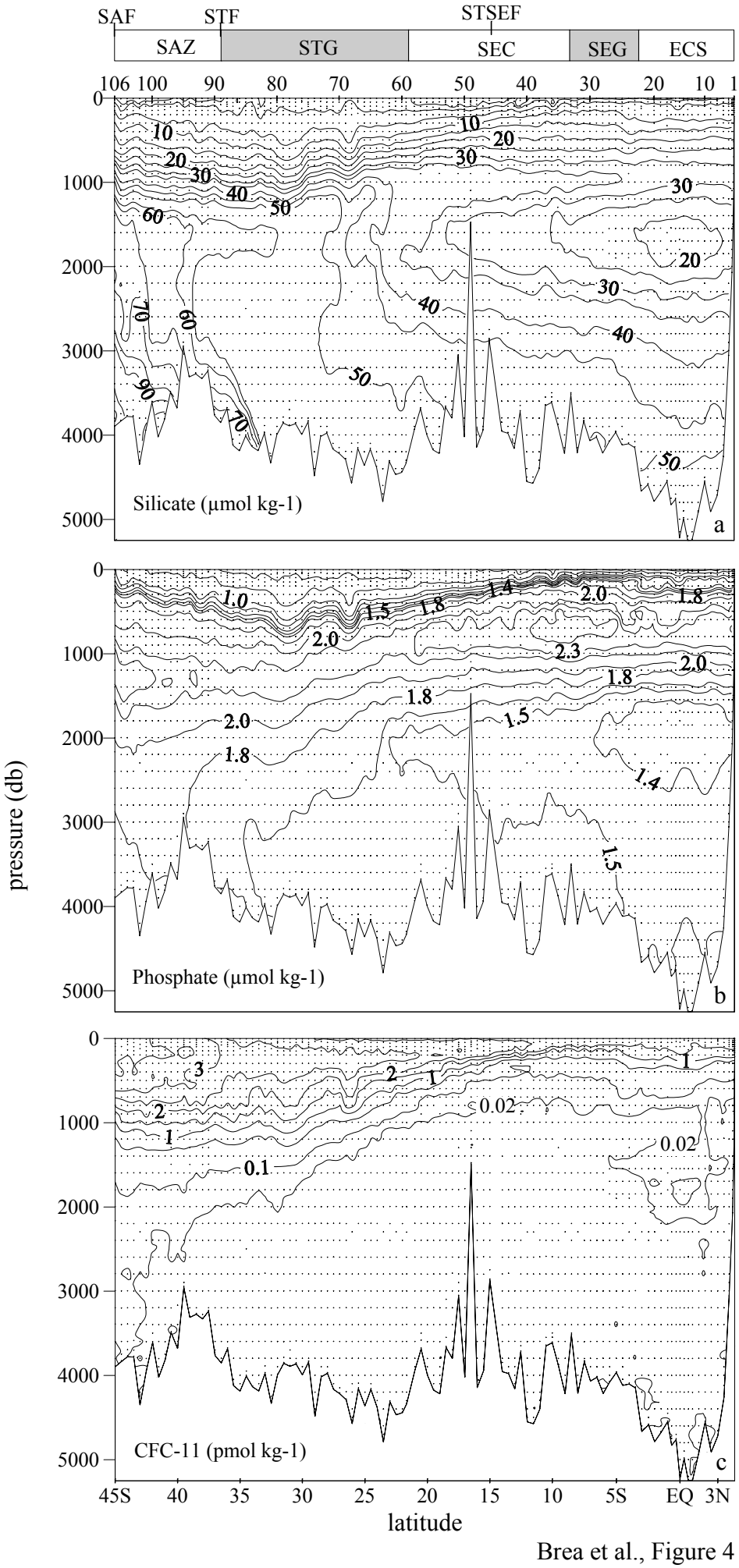

Brea et al., Figure 4

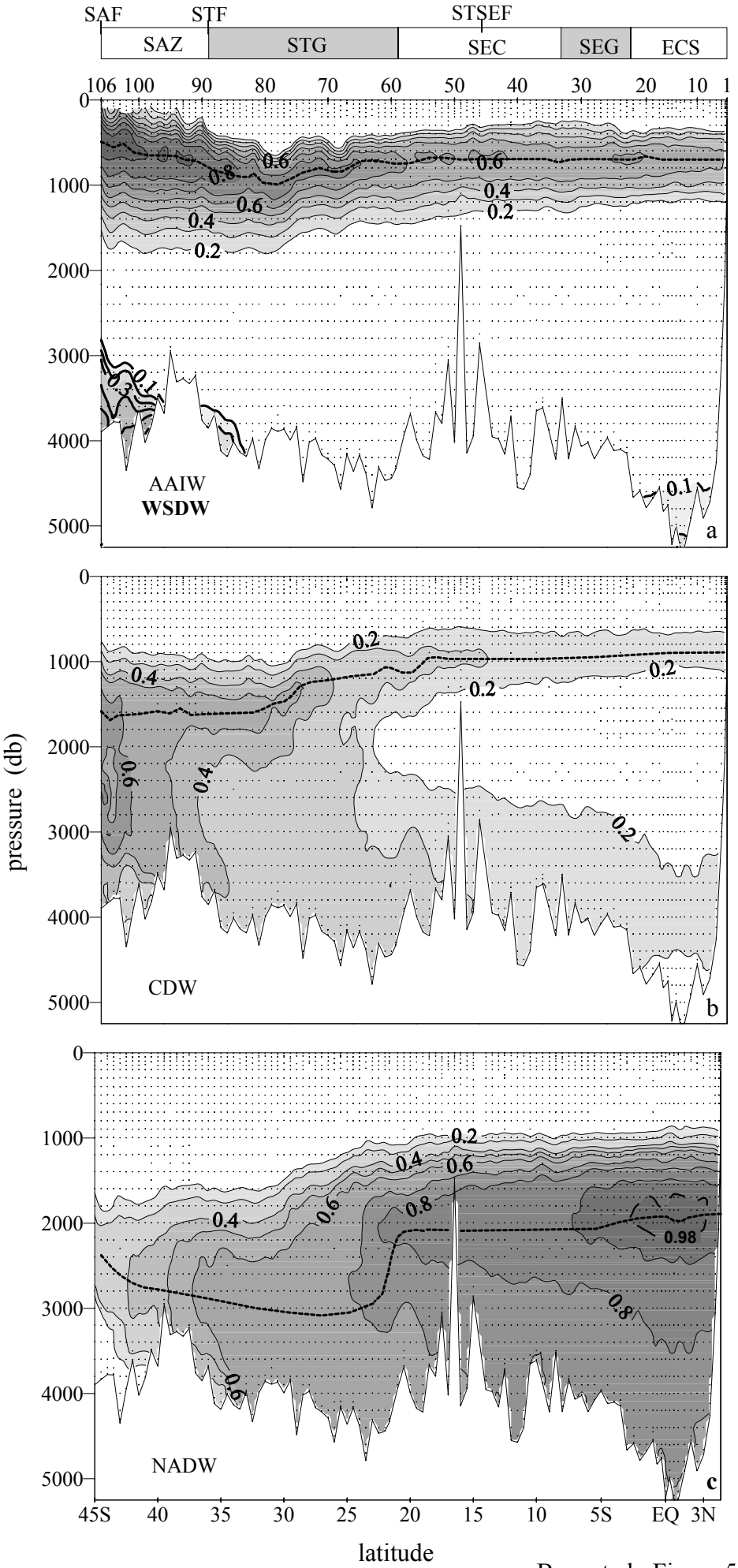

Brea et al., Figure 5

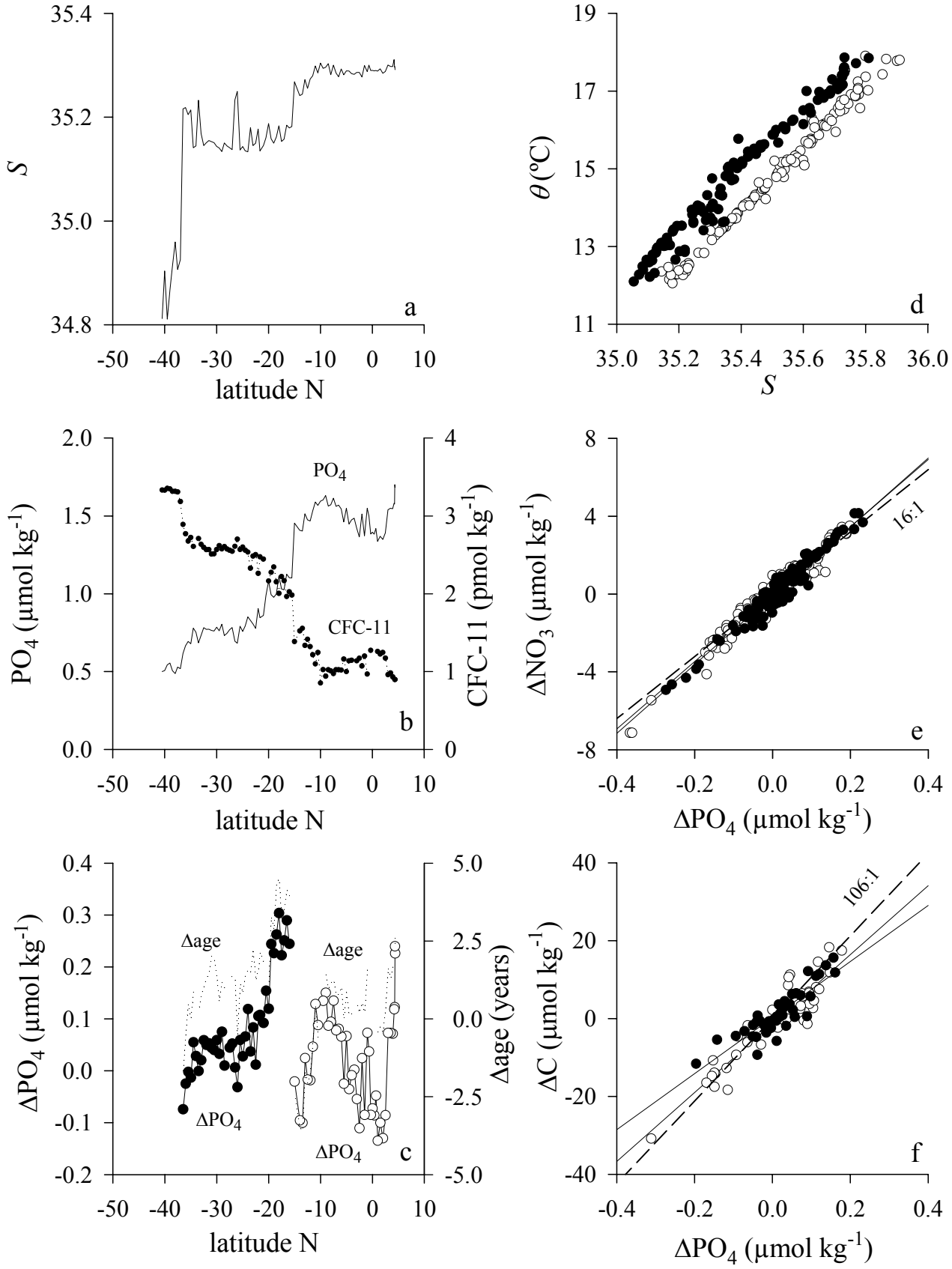

Brea et al., Figure 6

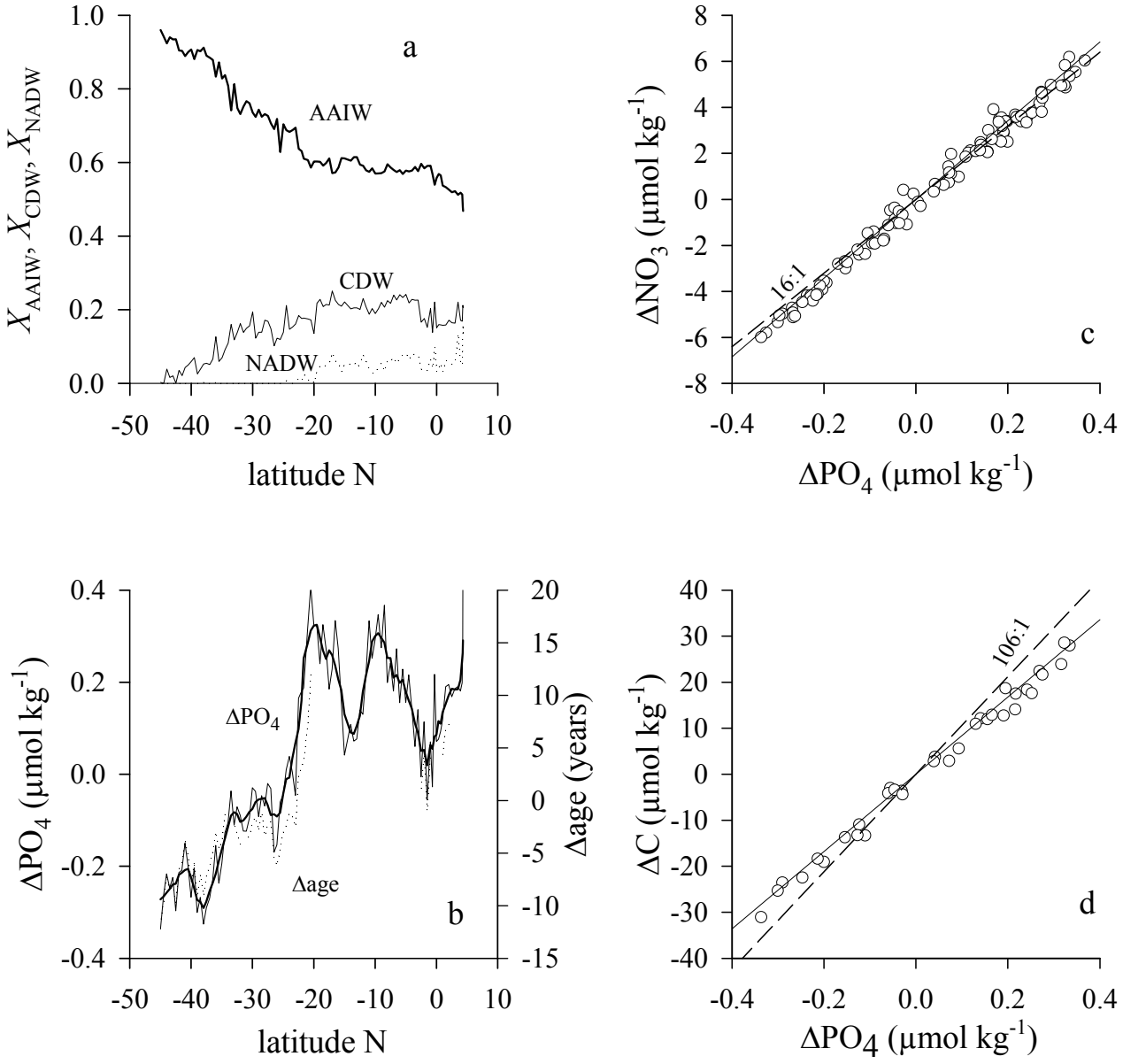

Brea et al., Figure 7

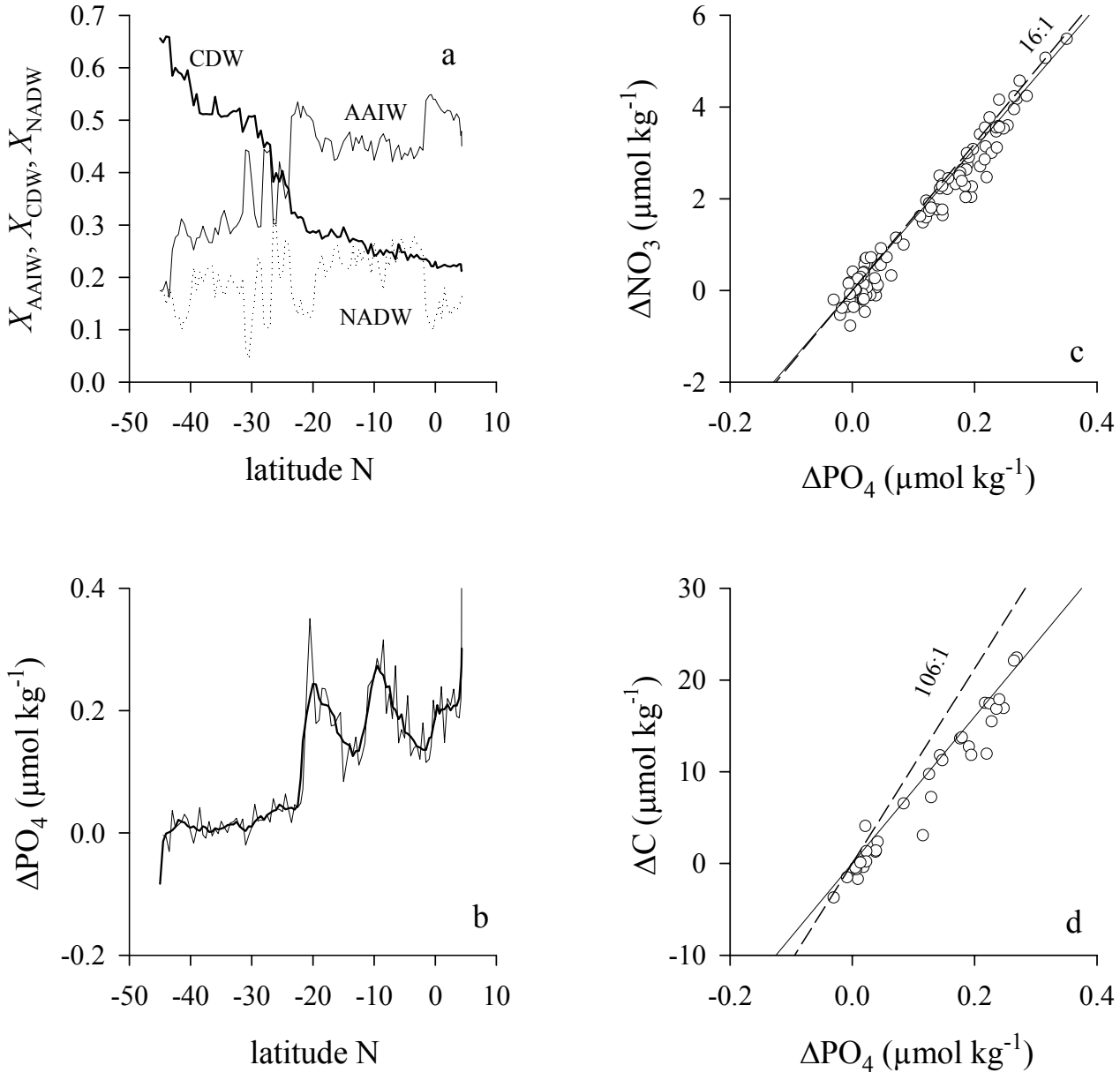

Brea et al., Figure 8

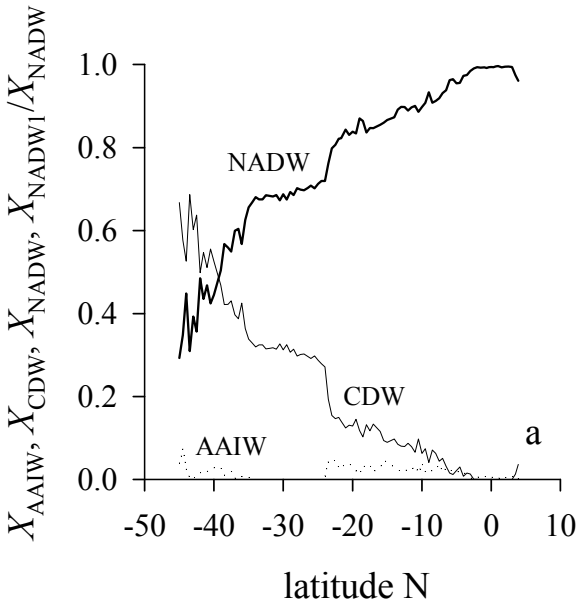

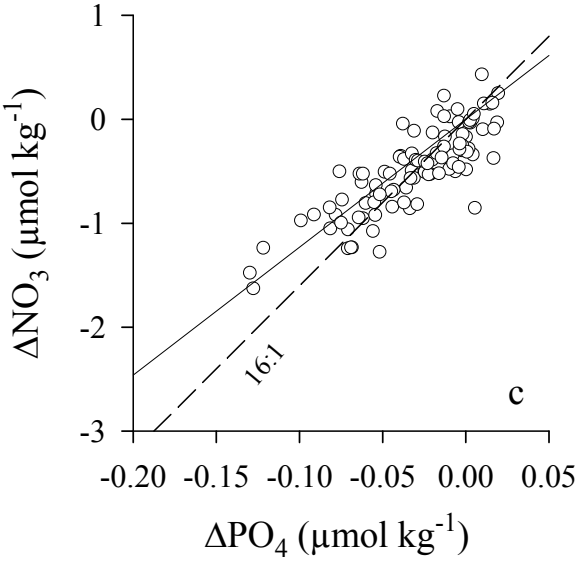

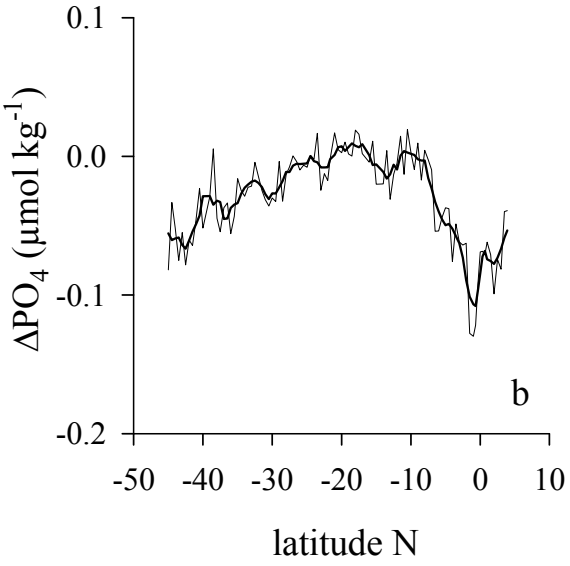

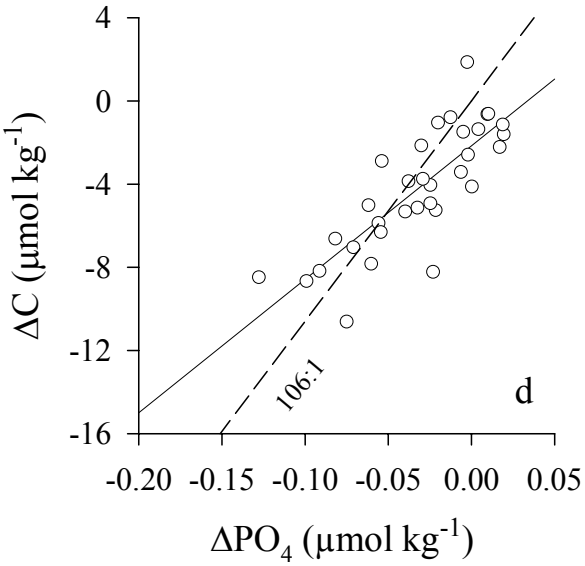

Brea et al., Figure 9

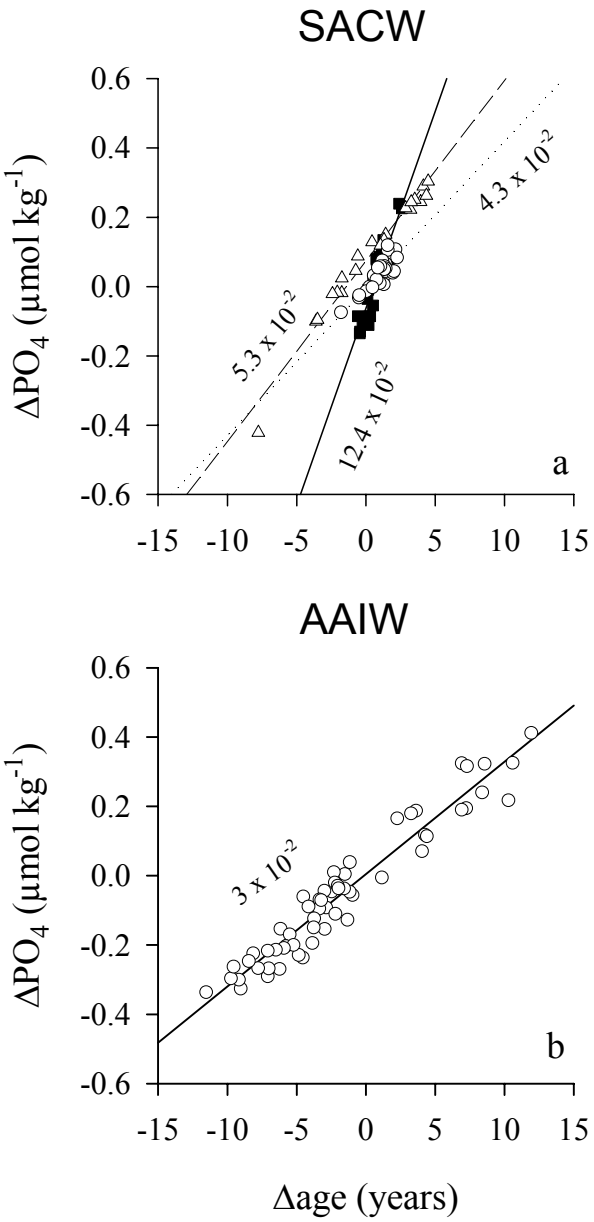

Brea et al., Figure 10